

## NUCLEAR RESONANCE IN EuS FROM 4.2°K TO THE CRITICAL TEMPERATURE REGION\*

P. Heller and G. Benedek

Department of Physics, Massachusetts Institute of Technology, Cambridge, Massachusetts

(Received 18 December 1964)

Nuclear magnetic resonance (nmr) can provide very accurate information on magnetic systems. The zero-field nmr frequency  $\nu$  gives the temperature dependence of the magnetization through the relation

$$M(T)/M(0) = \nu(T)/\nu(0). \quad (1)$$

For the antiferromagnet  $\text{MnF}_2$  we have shown<sup>1</sup> how nmr can provide a highly detailed and precise account of the magnetic ordering process near the critical temperature  $T_c$ . Recent theoretical developments<sup>2-4</sup> make it particularly important to extend this work to ferromagnets, especially to the insulators in which the magnetic electrons are localized at the lattice sites. Of these systems, the compound<sup>5</sup> EuS is ideal because of its cubic structure and the spin-only moment of the  $\text{Eu}^{++}$  ion.

The europium nuclear resonances in ferromagnetic EuS were first studied by Charap and Boyd<sup>6</sup> from 1.9 to 4.2°K. We now report accurate measurements of the zero-field nuclear resonance frequencies in EuS powder from 4.2 to 16.33°K. The Curie point  $T_c$  is at 16.5°K. In this Letter, while we emphasize the critical region, we present data of vital importance for a detailed examination of spin-wave interaction theories.<sup>7,8</sup>

Nuclear resonances were observed with a frequency-modulated Kushida spectrometer<sup>9</sup> operating up to 210 Mc/sec. The temperature was Servo controlled to within a millidegree. A temperature sweep was achieved by continuously varying the reference resistor in the Servo loop. The nmr lines were displayed at fixed frequency by sweeping the temperature. The usual swept-frequency method proved impractical because of the very large linewidths.

Temperatures were measured with a germanium resistance thermometer, calibrated as follows: (a) For 10°K  $< T < 20$ °K it was compared with a platinum resistance thermometer read with the aid of a  $Z$  function.<sup>10</sup> (b) For the important region 14°K  $< T < 17$ °K, it was compared with a hydrogen vapor-pressure thermometer whose bulb was situated at the position of the EuS sample; hydrogen vapor pressures were converted to absolute temperatures with the formulas of Wooley, Scott, and Brick-

wedde.<sup>11</sup> In addition, it was calibrated (c) at the superconducting transition,<sup>12</sup> 7.193°K, of a very pure lead sample and (d) in liquid helium at 4.21°K. For  $T \leq 10$ °K, a scale of thermometer resistance versus temperature was constructed analytically to fit (c), (d), and (a). This scale was then checked (e) by observing the  $\text{Cr}^{53}$  nuclear resonance in  $\text{CrBr}_3$  and comparing with Narath's data.<sup>13</sup> The reproducibility and consistency of these methods indicate that our calibration is accurate to within  $\pm 0.04$ °K for  $T < 14$ °K and  $\pm 0.02$ °K for  $T > 14$ °K.

The nmr data obtained are presented in Table I. The uncertainties given describe the precision in locating the center of the lines. Resonances for both the  $\text{Eu}^{153}$  and  $\text{Eu}^{151}$  nuclei were observed. The relatively narrow  $\text{Eu}^{153}$  line was studied in detail. The reduced magnetization is obtained from Table I(a) by using (1) together with Charap and Boyd's result

$$\nu^{153}(0) = 151.6 \text{ Mc/sec.} \quad (2)$$

To make contact with theoretical discussions<sup>3</sup> we fit our data to the equation

$$\nu(T)/\nu(0) = D(1 - T/T_c)^\beta. \quad (3)$$

Equation (3) should hold asymptotically as  $T \rightarrow T_c$ . To make the fit we find a value of  $\beta$  for which  $\nu^{1/\beta}$  is linear in temperature near  $T_c$ . That the choice  $\beta = \frac{1}{3}$  is a good one is shown dramatically in Fig. 1, where we plot  $\nu^3$  versus  $T$ . To find the precision with which the data define  $\beta$ , we put

$$\Delta T = (T_c - T) - T_c \left\{ (1/D) [\nu(T)/\nu(0)] \right\}^{1/\beta}, \quad (4)$$

and plot  $\Delta T/T_c$  versus  $T/T_c$  for five choices of  $\beta$  as shown in Fig. 2. Then the region in which (3) applies is the one in which the plot of  $\Delta T/T_c$  has no curvature.

Figure 2 shows that the data fit (3) for  $0.9T_c < T < 0.99T_c$  with

$$\beta = 0.33 \pm 0.015. \quad (5)$$

The uncertainty quoted in (5) includes our estimate of the precision in determining the shape of the thermometer calibration curve in the

Table I. Temperature dependence of  $\text{Eu}^{153}$  and  $\text{Eu}^{151}$  resonances in ferromagnetic  $\text{EuS}$ .

Temperature, $T$ (°K)	Frequency, $\nu$ (Mc/sec)	Temperature, $T$ (°K)	Frequency, $\nu$ (Mc/sec)
(a) $\text{Eu}^{153}$		(a) $\text{Eu}^{153}$	
4.21 ± 0.03	146.76	14.193 ± 0.005	90.08
4.91 ± 0.02	144.74	14.571 ± 0.005	84.94
5.20 ± 0.02	143.86	14.864 ± 0.005	80.70
5.37 ± 0.02	143.33	15.184 ± 0.005	74.97
5.98 ± 0.02	141.37	15.481 ± 0.005	68.93
6.20 ± 0.015	140.69	15.754 ± 0.007	62.22
6.55 ± 0.015	139.43	15.979 ± 0.007	55.08
7.23 ± 0.015	136.96	16.000 ± 0.007	54.16
7.75 ± 0.015	134.76	16.025 ± 0.007	53.23
8.16 ± 0.015	133.09	16.026 ± 0.007	53.26
8.66 ± 0.015	130.80	16.079 ± 0.007	51.21
9.20 ± 0.015	128.15	16.183 ± 0.007	46.57
9.69 ± 0.015	125.58	16.236 ± 0.007	43.60
10.27 ± 0.015	122.46	16.271 ± 0.010	42.10
10.82 ± 0.015	119.07	16.311 ± 0.010	38.81
11.21 ± 0.015	116.59	16.333 ± 0.012	37.95
11.74 ± 0.015	113.01		
11.94 ± 0.010	111.43	(b) $\text{Eu}^{151}$	
12.00 ± 0.010	111.08	14.04 ± 0.015	207.00
12.35 ± 0.010	108.32	14.765 ± 0.015	184.23
12.773 ± 0.007	104.77	15.56 ± 0.02	150.60
13.105 ± 0.007	101.80	15.765 ± 0.02	138.35
13.681 ± 0.007	96.12	15.985 ± 0.025	123.15
14.135 ± 0.005	90.81	16.13 ± 0.025	109.65
		16.175 ± 0.025	105.67

critical region. We also conclude that

$$T_c = (16.50 \pm 0.03)^\circ\text{K}, \text{ and } D = 1.145 \pm 0.02. \quad (6)$$

The uncertainties in (6) are mainly due to the uncertainty in  $\beta$ .

Our conclusions regarding the critical behavior have been drawn from data extending up to  $0.99T_c$ , where  $\nu/\nu(0) = \frac{1}{4}$ . Rapid fading of the nuclear resonance together with a strongly temperature-dependent electronic absorption made measurements nearer  $T_c$  extremely difficult. While one may question the applicability of (5) and (6) in the temperature range  $0.99T_c < T < T_c$ , we must point out that for the case of the measurements<sup>1</sup> on  $\text{MnF}_2$ , which extended up to  $0.99993T_c$ , omission of the data for  $T > 0.99T_c$  does not affect<sup>14</sup> the value deduced for  $\beta$ .

In a low-anisotropy material such as  $\text{EuS}$ , the precession of the nuclear polarization can strongly perturb the electronic magnetization. DeGennes *et al.*<sup>15</sup> showed how this can lead to a "pulling" of the nmr frequency by an amount

$\delta\nu$  given by

$$\delta\nu/\nu = -mH_n/MH_A. \quad (7)$$

Here  $\nu$  is the nmr frequency in the absence of pulling,  $m$  and  $M$  are the static nuclear and electronic magnetizations,  $H_n$  is the static field at the nucleus, and  $H_A$  is the anisotropy

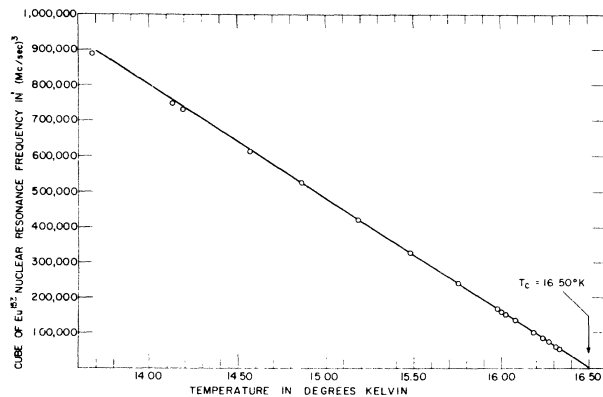


FIG. 1. Temperature dependence of the cube of the  $\text{Eu}^{153}$  nuclear resonance frequency between 13.6 and  $16.33^\circ\text{K}$ . We see that the law  $\nu(T)/\nu(0) = D(1 - T/T_c)^{1/3}$  holds very well for the range  $14.9^\circ\text{K} < T < 16.33^\circ\text{K}$ .

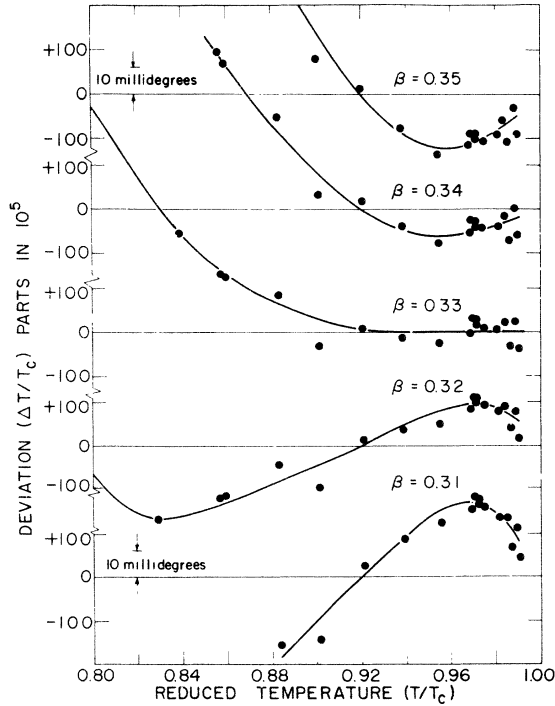


FIG. 2. Deviations from Eq. (3) for five choices of  $\beta$ . The most appropriate choice is the one for which the plot of  $\Delta T/T_c$  vs  $T/T_c$  has no curvature as  $T \rightarrow T_c$ . The quantity  $\Delta T$  is defined by Eq. (4). It represents the departure in temperature of a  $\nu^{1/\beta}$ -vs- $T$  plot from a straight line.

field. For the  $\text{Eu}^{153}$  nuclei in  $\text{EuS}$ , Eq. (7) becomes approximately

$$\delta\nu^{153}/\nu^{153} = -0.16(TH_A)^{-1}M(T)/M(0), \quad (8)$$

with  $T$  in  $^\circ\text{K}$  and  $H_A$  in gauss. Thus the pulling effect could become appreciable at very low temperatures, or just below  $T_c$  where  $H_A$  is small.

We now show how this effect can be detected and corrected for by observing the ratio of the observed frequencies of the two europium isotopes,

$$R = \left( \frac{\nu^{151}}{\nu^{153}} \right)_{\text{obs}} = \frac{\nu^{151} + \delta\nu^{151}}{\nu^{153} + \delta\nu^{153}}. \quad (9)$$

Let  $R_0 = \nu^{151}/\nu^{153}$  denote the value of this ratio in the absence of pulling. Since the two isotopes have equal spins and nearly equal abundances,

$$\frac{\delta\nu^{151}/\nu^{151}}{\delta\nu^{153}/\nu^{153}} = \frac{m^{151}}{m^{153}} = \left( \frac{\gamma^{151}}{\gamma^{153}} \right)^2 = R_0^2.$$

Then (9) yields

$$R = R_0 + \Delta R, \quad (10)$$

where

$$\Delta R = R_0(R_0^2 - 1)(\delta\nu^{153}/\nu^{153}). \quad (11)$$

For  $2.5^\circ\text{K} < T < 4.2^\circ\text{K}$ , Charap and Boyd<sup>16</sup> found  $R = 2.262 \pm 0.002$ , independent of temperature. Since  $\Delta R \sim 1/T$ , the observed constancy of  $R$  implies that

$$R_0 = 2.262. \quad (12)$$

Using (10), (11), and (12),  $\delta\nu^{153}/\nu^{153}$  was calculated for each temperature at which the  $\text{Eu}^{151}$  resonance was recorded, enabling us to determine the extent of the nuclear pulling. From these calculations we found that the pulling effects on the  $\text{Eu}^{153}$  resonance frequencies listed in Table I(a) are quite small, being at worst comparable to the accompanying experimental uncertainties. Furthermore, correction for the pulling can only shift the exponent  $\beta$  slightly upward by an amount  $\delta\beta = 0.005 \pm 0.005$ .

We are greatly indebted to Dr. J. S. Smart and Dr. M. W. Shafer of the IBM Watson Research Center for kindly providing the  $\text{EuS}$  samples.

\*Research supported by the Advanced Research Projects Agency under Contract No. SD 90.

<sup>1</sup>P. Heller and G. B. Benedek, *Phys. Rev. Letters* **8**, 428 (1962).

<sup>2</sup>G. A. Baker, Jr., *Phys. Rev.* **124**, 767 (1961).

<sup>3</sup>J. W. Essam and M. E. Fisher, *J. Chem. Phys.* **38**, 802 (1963).

<sup>4</sup>J. Gammel, W. Marshall, and L. Morgan, *Proc. Roy. Soc. (London)* **A275**, 257 (1963).

<sup>5</sup>T. R. McGuire, B. E. Argyle, M. W. Shafer, and J. S. Smart, *Appl. Phys. Letters* **1**, 17 (1962).

<sup>6</sup>S. H. Charap and E. L. Boyd, *Phys. Rev.* **133**, A811 (1964).

<sup>7</sup>F. J. Dyson, *Phys. Rev.* **102**, 1217, 1230 (1956).

<sup>8</sup>M. Bloch, *Phys. Rev. Letters* **9**, 286 (1962).

<sup>9</sup>G. B. Benedek and T. Kushida, *Phys. Rev.* **118**, 46 (1960).

<sup>10</sup>G. K. White, *Experimental Techniques in Low-Temperature Physics* (Oxford University Press, New York, 1959), p. 114.

<sup>11</sup>H. W. Woolley, R. B. Scott, and F. G. Brickwedde, *J. Res. Nat. Bur. Stand.* **41**, 379 (1948).

<sup>12</sup>J. P. Franck and D. L. Martin, *Can. J. Phys.* **39**, 1320 (1961).

<sup>13</sup>H. L. Davis and Albert Narath, *Phys. Rev.* **134**, A433 (1964).

<sup>14</sup>P. Heller and G. B. Benedek, International Conference on Magnetism, Nottingham, U. K., September 1964 (unpublished).

<sup>15</sup>P. G. DeGennes, P. A. Pincus, F. Hartmann-Boutron, and J. M. Winter, Phys. Rev. 129, 1105

(1963).

<sup>16</sup>E. L. Boyd, private communication.

### SMALL-ANGLE ELASTIC SCATTERING OF HIGH-ENERGY PROTONS FROM HYDROGEN\*†

K. J. Foley, R. S. Gilmore,‡ R. S. Jones, S. J. Lindenbaum, W. A. Love, S. Ozaki, E. H. Willen, R. Yamada, and L. C. L. Yuan  
Brookhaven National Laboratory, Upton, New York  
(Received 22 December 1964)

We present the results of an experiment performed at the Brookhaven AGS to measure high-energy  $p$ - $p$  scattering in the range of laboratory angle 2 to 20 mrad. Elastic scattering events were separated by momentum analysis. The prime purpose of the experiment was to investigate Coulomb interference effects. The range of incident particle momentum studied was 8 to 18 BeV/ $c$ .

The apparatus is shown in Fig. 1. A small-angle secondary beam from the AGS was momentum analyzed ( $\pm 0.8\%$  half-width at half-maximum) and focused on a liquid hydrogen target 18 in. long and 4 in. in diameter. The beam was defined by the scintillation counter S2 and the scintillation counter hodoscopes HO2 and HO3. The incident particle was selected by the differential Cherenkov counter C, and its angle was measured to  $\pm 0.3$  mrad (half-width at half-maximum) by HO2 and HO3. Each hodoscope was made up of  $\frac{1}{4}$  in. wide scintillation counters in 4-element  $\times$  4-element two-dimensional arrays. The hodoscopes HO2, HO3, and H2 determined the horizontal projection of the scattering angle to  $\pm 0.4$  mrad while HO2, HO3, and H4 determined the vertical projection to  $\pm 0.4$  mrad. The momentum of the final particle was measured to  $\pm 0.8\%$  with HO3, H2, and H4. Hodoscope H2 comprised 80 counters, each  $\frac{1}{4}$  in. wide  $\times$  6 in. high. The 120 vertical elements of H4 were each  $\frac{1}{2}$  in. wide  $\times$  13 in. high and the 24 horizontal elements were each  $\frac{1}{2}$  in. high  $\times$  61 in. long. The absolute

mean momentum of the incident particles was determined to within 0.2%.

The trigger system included the counters L2 and the sum of the outputs of the vertical elements in H4. L2 excluded the unscattered beam and H4 limited the range of momentum of the scattered particle. On a fast ( $\sim 20$ -nsec) coincidence between these counters and a selected beam particle, 192 fast discriminator gates ( $\sim 40$  nsec) were opened and signals were detected from those counters which had fired. This information was then transferred to a buffer memory and, approximately 15  $\mu$ sec later, the system was ready to accept another event. A signal from a ring counter (ANTI) behind the hodoscope HO2 was fed into the buffer memory at the same time so that the program could reject those events with an extra particle passing through the collimator but outside of HO2. The data-handling system was similar in principle to that described in earlier publications.<sup>2</sup> However, a new buffer memory with about 65 times the capacity<sup>3</sup> of the early system was used to take advantage of the high event rates available in this experiment. At the end of an AGS burst the information stored in the memory was transferred in parallel to magnetic tape and, via coaxial cables, to the Merlin computer. During the runs the computer analyzed events and stored them in a two-dimensional array of events versus angle and momentum of the scattered particle. At the end of each run the computer subtracted the inelastic background by linear interpolation and calculated the differential cross section. Unfortunately, the data-handling capacity of Merlin was inadequate at the high event rates, which at times exceeded  $10^6$ /hour, so the data analysis was completed using the BNL IBM 7094. The Merlin analysis served as a monitor during the experiment, providing immediate feedback via scope display and printouts.

The target-empty background varied from

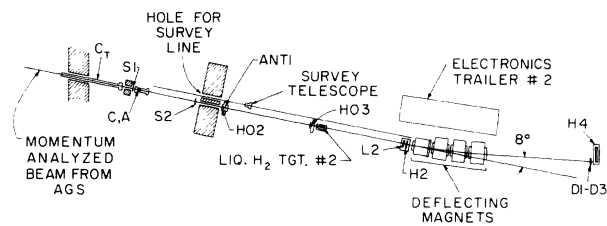


FIG. 1. The experimental arrangement.